Experimental study on the web crippling behaviour of pultruded GFRP channel sections using DIC

Li-Teng Zhang[1] *and Chao Wu*[1,*]
[1]*School of Transportation Science and Engineering, Beihang University, 37 Xueyuan Road, Beijing 100191, China*
Corresponding author: wuchao@buaa.edu.cn

Abstract. The use of pultruded glass fibre reinforced polymer has gained wide acceptance in civil engineering due to their excellent physical and mechanical characteristics, like low weight, high strength and durability in harsh environment. However, duo to the pultrusion process, pultruded GFRP sections are orthotropic and face a critical issuse of web crippling. This paper presents an experimental study on the web crippling behavior of pultruded GFRP channel sections under transverse bearing load. A total of twenty specimens were tested under two loading conditions, namely end-two-flanges (ETF) and interior-two-flanges (ITF). Five different bearing plates with length ranging from 20 mm to 200 mm were chosen to apply the transverse concentrated loading. It is observed taht all specimens initially cracked at the web-falnge junction. The experimental result also confirmed that both the web crippling capacities and stiffness increased with the increase of the bearing length. And the web crippling capacities are improved when the bearing plates are moved from the end to the middle of the specimen. The strain distributions at the web-flange junction obtained by DIC indicated that both the materials underneath the bearing plates and that near the bearing plates engaged in carrying the transverse bearing load.

Keywords: Web crippling; pultruded; GFRP; Channel section; DIC

1 Introduction

Pultruded glass fiber reinforced polymer (GFRP) are seeing an increasing application in civil engineering due to their excellent physical and mechanical properties, like low weight, high strength and resistance to harsh environment [1,2]. However, because of their inherent pultrusion process, pultruded GFRP sections exhibited much lower mechanical properties in the transverse direction than that in the pultrusion direction. The highly orthotropic causes pultruded GFRP facing a critical issue of premature web crippling failure under transverse bearing load. In order to break the hinders of the widespread of pultruded GFRP sections in the practical civil constructions, many studies [3,4] were conducted on the web crippling behavior of pultruded GFRP sections. Wu and Bai [4] creatively investigated the web crippling behavior of GFRP rectangle hollow sections. The concentrated bearing loading was applied by four loading conditions of end-two-flange (ETF), interior-two-flange (ITF), end ground (EG) and interior ground (IG). It is found that the failure initiated at the web-flange junction and was followed by buckling or crushing in the web. Based on the out-off-plane displacement, a simple failure mechanism was proposed to predicte the strength of such GFRP sections subjected to web crippling. Similarly, Chen and Wang [5] and Fernandes et.al [6,7] also conducted a series of experimental studies on the web crippling behavior of pultruded GFRP I sections. Four different GFRP I sections with heights ranging from 100 mm to 400 mm were tested under ETF and ITF loading conditions. Three different bearing plate of 15 mm, 50 mm, 100 mm were chosen to apply the concentrated bearing loading. The result confirmed that when the bearing length was changed from 15 mm to 100 mm, the web crippling strength increased up to +139% and +230%, for the ITF and ETF load configurations, respectively, while the stiffness increased up to +129% and +224%, respectively. It should be noticed that the former studies focused on the web crippling behavior of symmetric sections. The asymmetric sections, such as channel sections, also play an important role in civil constructions. It is also necessory to investigate the web crippling bahavior of asymmetric sections. Zhang and Chen [8] reported the web crippling behavior of pultruded GFRP channel sections under ETF, ITF, EG

* Corresponding author: wuchao@buaa.edu.cn

and IG loading conditions. A main bending crack was clearly observed at the mid height of the web of all specimen. And the experimental result showed that the ultimate strength of the specimens with interior bearing load was all larger than those of the specimens with end bearing load. However, the studies on the web crippling behavior of channel sections are still limited, and many critical parameters like web slenderness ratio, specimen length, corner radius have not been considered.

As discussed earilier, the web crippling behavior of pultruded GFRP symmetric sections have been extensively studied. However, the knowledge of web crippling mechanism of asymmetric sections, such as channel section, is still limited. This paper presents an experimental study on the web crippling behavior of pultruded GFRP channel sections. One pultruded GFRP channel section was chosen for the web crippling test. Two loading conditions of end-two-flanges (ETF) and interior-two-flanges (ITF) were applied. Five different bearing lengths of 20 mm, 50 mm, 100 mm, 150 mm and 200 mm were chosen. The typical failure mode of web-flange junction failure was observed in all tested specimens. Load-displacement curves, web crippling capacities and stiffness were obtained by the web crippling test. The strain distributions at the web calculated by digital image correlation (DIC) were used to reveal the stress transferring mechanism at the crack initiation.

2 Experimental program

A total of twenty pultruded GFRP channel specimens were tested as shown in Table 2. All the specimens have a height of 102 mm, a width of 35 mm and a web/flange thickness of 4.8 mm using the symbol shown in Fig. 1. The specimen length was twice of the height of the web according to ASCE Specification [9] and the AS/NZS 4673 [10]. The specimen ID shown in Table 2 consists of three parts. The first part is the loading conditions of ETF and ITF. The second part represents the bearing length, i.e.20, 50, 100, 150, 200. The third part means the repeating times of each test. The coupons were cut from the centre of the web and tested for tensile properties according to ASTM D 3039 [11] and for interlaminar shear properties according to ASTM D 2344 [12]. The measured mechanical properties of GFRP sections were listed in Table 1.

Table 1. Mechanical properties of pultruded GFRP sections

Item	Tensile strength	Tensile modulus	Interla

Direction	Longitudinal $f_{t,L}$ (MPa)	Transverse $f_{t,T}$ (MPa)	Longitudinal $E_{t,L}$ (GPa)	Transverse $E_{t,T}$ (GPa)	minar shear strength τ (MPa)
Value	321.4	56.5	25.2	8.6	27.8

Table 2. Specimen and experimental result

Section ID	Web crippling capacity P_{exp} (kN)	Stiffness K (kN/mm)
ITF-20-1	9.93	7.1
ITF-20-2	9.71	7.0
ETF-20-1	5.52	3.1
ETF-20-2	7.52	3.0
ITF-50-1	17.90	14.7
ITF-50-2	15.26	14.5
ETF-50-1	11.04	9.2
ETF-50-2	13.66	9.2
ITF-100-1	27.06	20.2
ITF-100-2	27.92	20.1
ETF-100-1	26.09	19.0
ETF-100-2	26.47	18.9
ITF-150-1	32.72	21.3
ITF-150-2	39.87	21.1
ETF-150-1	27.19	19.4
ETF-150-2	30.60	19.6
ITF-200-1	46.56	23.6
ITF-200-2	45.24	23.6
ETF-200-1	40.93	22.0
ETF-200-2	46.08	22.1

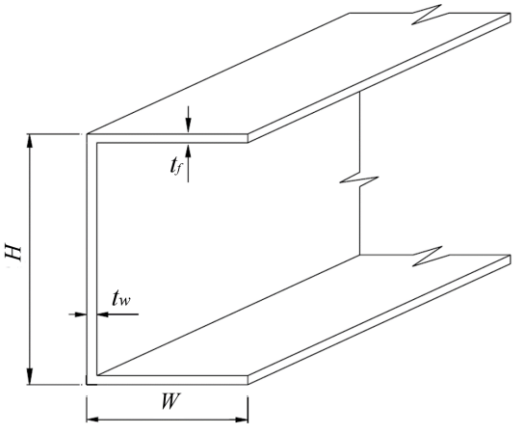

Fig. 1. Dimensions of the pultruded GFRP channel section

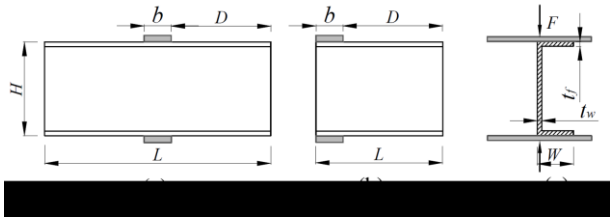

Fig. 2. (a) ITF; (b) ETF and (c) side view of the two loading conditions

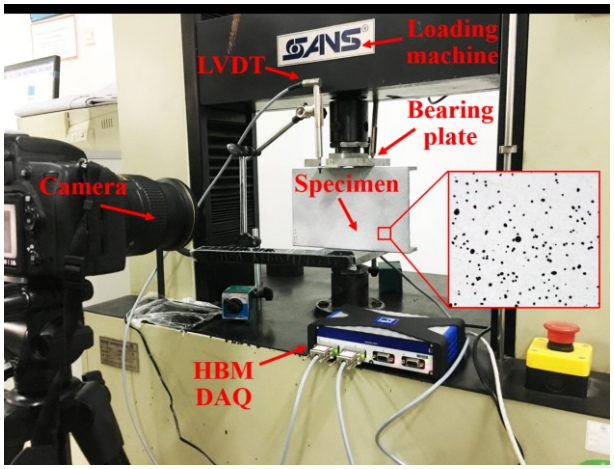

Fig. 3. Experimental setup and instrumentations

The loading conditions of ETF and ITF are shown in Fig. 2. The experimental setup is presented in Fig. 3. All the specimens were tested on a SANS universal test machine with the capacity of 100 kN. The load was applied by the bearing plates with a constant displacement control at a speed of 1 mm/min. The channel sections were placed between two bearing plates to make sure the transverse concentrated load through the centerline of the web. Two LVDTs were installed to measure the vertical displacement of each specimen. The specimens were painted with a speckle pattern on the surface for DIC analysis, produced by a thin coating of white paint followed by a uniformly distributed black dots using spray paint. A Nikon camera were setup to record the test process. And the photos were used for DIC analysis to calculate the strain distributions at the web. The detailed DIC method can be referred to [13].

3 Result and discussion

3.1. Failure mode

The typical failure modes of all specimen under different bearing plates are shown in Fig. 4-8, respectively. It was observed that the initial 45° cracking occurred at the web-flange junction for all specimen under both ETF and ITF loading conditions. During the compression process, the longitudinal cracks elongated alone the pultrusion direction and extended to zone beyond the area underneath bearing plates accompanying the increased of the transverse loading. The subsequently web buckling cracks were also observed following the initial web-flange junction failure with the loading increased as shown in Fig. 7(b).

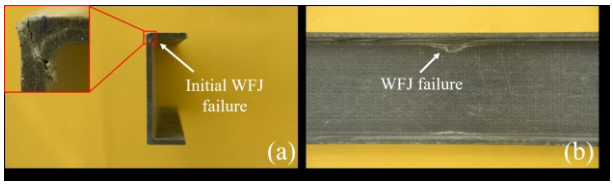

Fig. 4. Failure mode of specimens tested with 20 mm bearing plates under (a) ETF and (b) ITF loading conditions

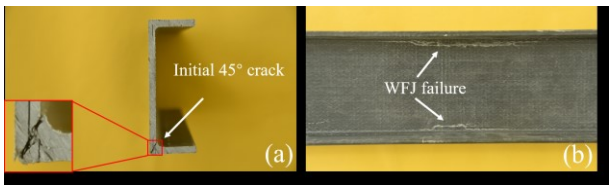

Fig. 5. Failure mode of specimens tested with 50 mm bearing plates under (a) ETF and (b) ITF loading conditions

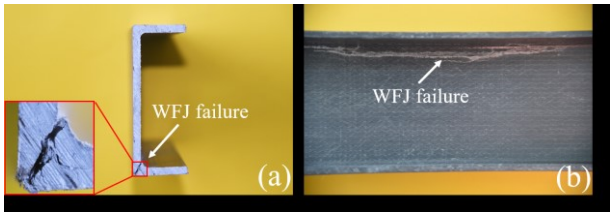

Fig. 6. Failure mode of specimens tested with 100 mm bearing plates under (a) ETF and (b) ITF loading conditions

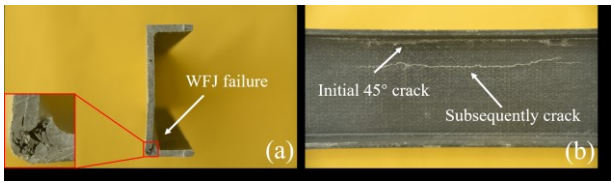

Fig. 7. Failure mode of specimens tested with 150 mm bearing plates under (a) ETF and (b) ITF loading conditions

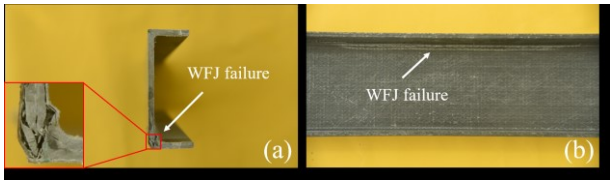

Fig. 8. Failure mode of specimens tested with 200 mm bearing plates under (a) ETF and (b) ITF loading conditions

3.2 Load-displacement curves and web crippling capacity

The load-displacement curves of the GFRP channel sections are presented in Fig. 9. For specimens subjected to ETF loading condition, the load linearly increased with the displacement upto a peak load at the first stage. And after the peak point, the load dropped suddenly to a lower level accompanying with a large cracking sound. And then, the subsequent non-linear curves indicated that the web continued to carry the transvers load. It is interesting to see that, for

specimen under ITF loading condition, the elastic linear stage was also observed in the beginning as shown in Fig. 9(b). Similar to specimens under ETF loading conditions, the channel sections under ITF loading conditions also exhibited a brittle failure after the peak load, expected for ITF-200 specimens. For ITF-200 specimen, the load gradually decreased after the peak load rather than a sudden drop.

The web crippling capacities were defined by the peak load corresponded to the curves shown in Fig. 9. The web crippling capacities of all specimens are presented in Table. 2 and Fig. 10. It is obvious that the web crippling capacities increased with the bearing length from 20 mm to 200 mm under both ETF and ITF loading conditions. As an example, increasing the bearing length from 20 mm to 200 mm led to the increase in the web crippling capacities by 367.4% (ITF) and 567.3% (ETF) under ITF and ETF loading conditions respectively. Besides, the web crippling capacities also increased when the bearing plates were moved from the end to the interior of the sections. For example, the largest increase by 50.6% were observed for specimens under 20 mm bearing plates, when the loading conditions were changed from ETF to ITF.

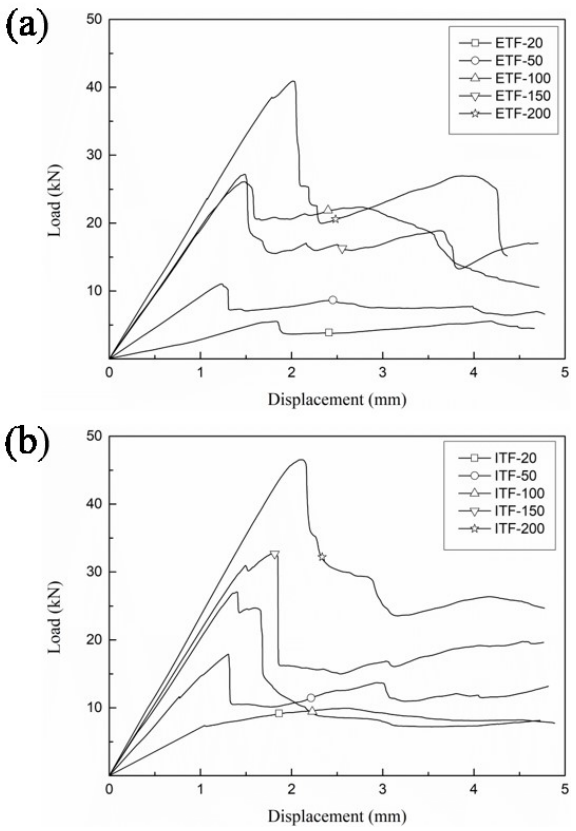

Fig. 9. Load-displacement curves for bearing length of 20 mm; 50 mm; 100 mm; 150 mm; 200 mm under (a) ETF and (b) ITF loading conditions

The stiffness of all specimens (slope of the linear stage in Fig. 9) was shown in Table. 2. As can be seen that the stiffness of GFRP sections increased with the length of bearing plates ranging from 20 mm to 200 mm subjected to both ETF and ITF loading conditions. A large increasing of 512.9% and 184.5% were observed for specimens subjected to ETF and ITF respectively, when the bearing length change from 20 mm to 100 mm, which were also confirmed in [6]. However, the stiffness almost shown no improvement when the bearing plates increased from 100 mm to 200 mm under both ETF and ITF loading conditions. This might relate to the stress concentration at the web-flange junction zone when the bearing length were less than 100 mm.

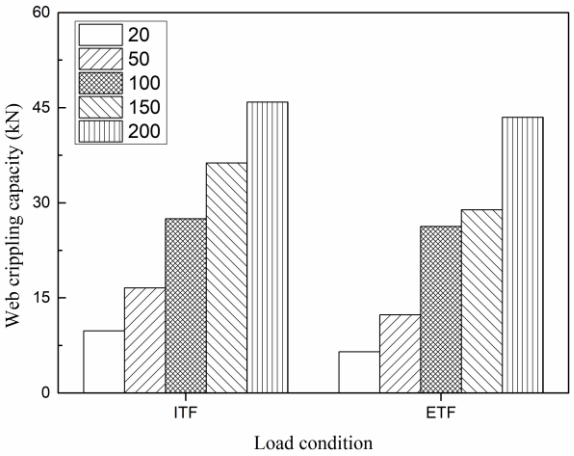

Fig. 10. Web crippling capacity of all tested specimens

3.3 Discussion on the failure mechanism with DIC

The typical strain distributions obtained by DIC method are presented in Fig. 11. It should be noted that the strain distributions correspond to the moment of initial failure and represent the transverse strain at the web. It is obvious that only a certain effective region (red area) underneath the bearing plates was activated to carry the transverse bearing loading. And the strain at other region (blue area) was almost zero, indicating the materials at blue area not contribute to carry the transverse load transferred from the bearing plates.

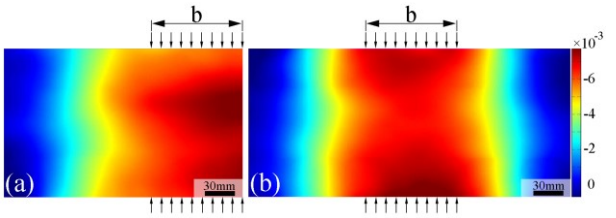

Fig. 11. Typical strain distributions at the web of specimen under (a) ETF and (b) ITF loading conditions

The strain distributions at the web-flange junction of all specimen were plotted in Fig. 12 for ETF and ITF loading conditions. And the strain curves were normalized by their corresponding peak strain. It can be seen that the strain curves at the initial web-flange junction were Parabola distribution. And the strain almost vanished at the zone away from the edge of the bearing plate. It indicates that, both the materials underneath the bearing plates and that near the bearing plates were activated to carry the transverse concentrated bearing load.

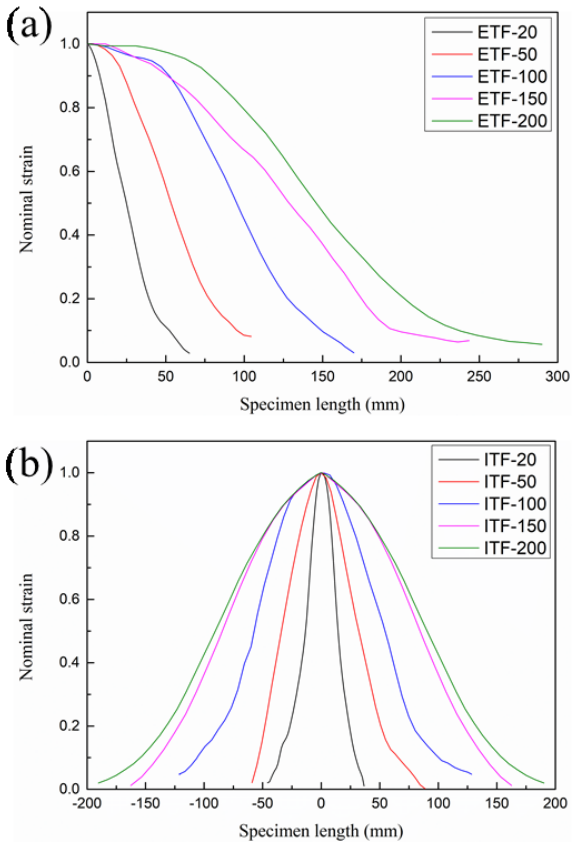

Fig. 12. Strain distribution curves at the initial web-flange junction failure of specimens under (a) ETF and (b) ITF loading conditions

4 Conclusion

This paper studied the web crippling behaviour of pultruded GFRP channel sections under transverse bearing load. A total of twenty specimens were conducted under both ETF and ITF loading conditions. Five different bearing plates with length ranging from 20 mm to 200 mm were chosen to apply the transverse concentrated load. The failure modes, load-displacement curves and web crippling capacities were presented. The stress transferring mechanism at the web-flange junction was extracted based on the strain distribution images obtained by DIC. And the following conclusions can be draw from the experimental result:

(1) The initial 45° crack was observed at the web-flange junction in all tested specimens, followed by the subsequently web buckling failure at the web.

(2) The web crippling capacities increased by 367.4% (ITF) and 567.3% (ETF) under ITF and ETF loading conditions respectively, when the bearing plate length changed from 20 mm to 200 mm. In addition, the web crippling capacities also exhibited a notable increasing when the bearing plates were moved from the end to the interior of the sections.

(3) The materials both underneath the bearing plates and near the bearing plates were contributed to carry the transverse bearing load.

Acknowledgement

The authors gratefully acknowledge the financial support provided by the National Science Foundation of China (51608020). This work was also funded by the Thousand Talents Plan (Young Professionals) in China.

References

1. Pendhari S S, Kant T, Desai Y M. Application of polymer composites in civil construction: A general review[J]. Composite Structures, 2008, 84(2):114-124.
2. Bank L C. Composites for construction: structural design with FRP materials. Design, 2006.
3. Chen Y, Wang C. Web crippling behavior of pultruded GFRP rectangular hollow sections[J]. Composites Part B Engineering, 2015, 77:112-121.
4. Wu C, Bai Y. Web crippling behaviour of pultruded glass fibre reinforced polymer sections[J]. Composite Structures, 2014, 108(1):789-800.
5. Chen Y, Wang C. Test on pultruded GFRP I-section under web crippling[J]. Composites Part B Engineering, 2015, 77:27-37.
6. Fernandes L A, Gonilha J, Correia J R. Web-crippling of GFRP pultruded profiles. Part 1: Experimental study[J]. Composite Structures, 2015, 120:565-577.
7. Fernandes L A, Nunes F, Silvestre N. Web-crippling of GFRP pultruded profiles. Part 2: Numerical analysis and design[J]. Composite Structures, 2015, 120:578-590.

8. Zhang W, Chen Y. Tests on GFRP pultruded profiles with channel section subjected to web crippling[J]. Applied Composite Materials, 2017, 24(4):1-14.
9. SEI/ASCE-8-02. Specification for the design of cold-formed stainless steel structural members[S]. Reston, VA, 1991.
10. AS/NZS 4673-2001. Cold-formed stainless steel structures[S]. Sydney, Australia, 2001.
11. ASTM D3039/D3039M-08, Standard test method for tensile properties of polymer matrix composite mterials[S]. United States, 2000.
12. ASTM D2344/D2344M-00, Standard test method for short-beam strength of polymer matrix composite materials and their laminates[S]. United States, 2006.
13. Ghiassi B. Application of digital image correlation in investigating the bond between FRP and masonry[J]. Composite Structures, 2013, 106(12): 340-349.